



## OPEN ACCESS

## EDITED BY

Wenqin Luo,  
Huzhou University, China

## REVIEWED BY

Renren Deng,  
Zhejiang University, China  
Wei Zheng,  
Fujian Institute of Research on the  
Structure of Matter, Chinese Academy  
of Sciences (CAS), China

## \*CORRESPONDENCE

Rute A. S. Ferreira,  
rferreira@ua.pt  
Carlos D. S. Brites,  
carlos.brites@ua.pt

## SPECIALTY SECTION

This article was submitted to Light  
Sources and Luminescent Materials,  
a section of the journal  
Frontiers in Photonics

RECEIVED 03 August 2022

ACCEPTED 14 September 2022

PUBLISHED 29 September 2022

## CITATION

Zanella S, Trave E, Moretti E, Talon A,  
Back M, Carlos LD, Ferreira RAS and  
Brites CDS (2022), Designing Ln<sup>3+</sup>-  
doped BiF<sub>3</sub> particles for luminescent  
primary thermometry and  
molecular logic.  
*Front. Photonics* 3:1010958.  
doi: 10.3389/fphot.2022.1010958

## COPYRIGHT

© 2022 Zanella, Trave, Moretti, Talon,  
Back, Carlos, Ferreira and Brites. This is  
an open-access article distributed  
under the terms of the [Creative  
Commons Attribution License \(CC BY\)](#).  
The use, distribution or reproduction in  
other forums is permitted, provided the  
original author(s) and the copyright  
owner(s) are credited and that the  
original publication in this journal is  
cited, in accordance with accepted  
academic practice. No use, distribution  
or reproduction is permitted which does  
not comply with these terms.

# Designing Ln<sup>3+</sup>-doped BiF<sub>3</sub> particles for luminescent primary thermometry and molecular logic

Sofia Zanella<sup>1</sup>, Enrico Trave<sup>2</sup>, Elisa Moretti<sup>2</sup>, Aldo Talon<sup>2</sup>,  
Michele Back<sup>2</sup>, Luís D. Carlos<sup>1</sup>, Rute A. S. Ferreira<sup>1\*</sup> and  
Carlos D. S. Brites<sup>1\*</sup>

<sup>1</sup>Phantom-g, CICECO-Aveiro Institute of Materials, Physics Department, University of Aveiro, Aveiro, Portugal, <sup>2</sup>Department of Molecular Sciences and Nanosystems, Ca' Foscari University of Venice, Venice, Italy

The design of molecular materials suitable for disparate fields could lead to new advances in engineering applications. In this work, a series of Ln<sup>3+</sup>-doped BiF<sub>3</sub> sub-microparticles were synthesized through microwave-assisted synthesis. The effects of doping are evaluated from the structural and morphological viewpoint. In general, increasing the Ln<sup>3+</sup> concentration the octahedral habitus is distorted to a spheric one, and some aggregates are visible without any differences in the crystalline phase. The optical response of the samples confirms that the BiF<sub>3</sub> materials are suitable hosts for the luminescence of the tested trivalent lanthanide (Ln<sup>3+</sup>) ions (Ln = Eu, Tb, Tm, Ho, Er, Yb). A Yb<sup>3+</sup>/Er<sup>3+</sup> co-doped sample is presented as an illustrative example of all-photonic molecular logic operations and primary luminescent thermometry.

## KEYWORDS

trivalent lanthanide, bismuth fluoride, luminescence, primary thermometry, molecular logic

## Introduction

The development of synthesis routes allowing the design of materials with virtually on-demand properties (*e.g.*, size, shape, functionality) is pivotal for cutting-edge applications in disparate research areas. It is well known that the morphology and size of the materials can impact their physical and chemical properties (Piana *et al.*, 2005; Alivisatos, 1996; Xia *et al.*, 2003), making engineered materials suitable for a wide range of applications. Trivalent lanthanide (Ln<sup>3+</sup>)-bearing materials have been widely investigated due to their distinctive high quantum yield (>50% in the visible spectral range, when incorporated in complexes), long-lived excited states (>1 ms), narrow emission bands (<10 nm), rendering versatility, and photostability, when incorporated in inorganic or organic-inorganic hosts (Bünzli, 2015). Ln<sup>3+</sup>-based materials attracted huge scientific scrutiny during the last 25 years for many optical applications from the development of solid-state lasers (Kuriki *et al.*, 2002), lightning (Bai *et al.*, 2014), displays (Chen *et al.*,

2013), and, in the last 10–15 years to luminescence nanothermometry (Jaue and Vetrone, 2012; Brites et al., 2019).

A relatively recent and sagacious application for  $\text{Ln}^{3+}$ -doped materials is molecular logic, which aims at developing molecular counterparts for current electronic logic systems (De Silva et al., 1993). Any physical and/or chemical change caused by an external stimulus (logic inputs) leading to a physical and/or chemical alteration of the material (logic output), may be interpreted as a transfer function connecting the logic inputs and outputs. Several materials have been designed to mimic the operation of conventional Boolean logic gates, demonstrating basic arithmetic functions and memory units (Erbas-Cakmak et al., 2018; Andréasson and Pischel, 2021; Nicoli et al., 2021). Converting the response of the luminescent material to the logical values 0 and 1, diverse logic gates can be defined. Molecular logic operations comprising chemical species as logic inputs and modifications on the photophysical properties (e.g., emission intensity, absorbance) as the output are those reported most often. Nevertheless, physical stimuli (e.g., light, temperature, pressure, magnetic field) may play the role of logic inputs, with many advantages such as no-contamination, reuse of the device, easy reconfiguration, and reprogramming (Andréasson et al., 2011; Brites et al., 2019; Zanella et al., 2022).

Irrespectively of the foreseen applications, to render tailorable photoluminescence response of the  $\text{Ln}^{3+}$ -doped materials, the host material should be precisely designed. Ideally, the host material would not interfere with the luminescence processes, therefore, host materials with low phonon energy are desirable. To date, fluorides, such as  $\text{NaYF}_4$  based materials have been widely investigated as luminescent host materials and remarkable results have been reported.  $\text{NaYF}_4$  has been used as a host in different contexts such as solar cells (Kumar et al., 2020), biodetection (Yi et al., 2004), detecting fingerprints (Xie et al., 2015), and display (Deng et al., 2015). As an alternative to the well-known  $\text{NaYF}_4$ , Bi-based matrices are an appealing candidate to host  $\text{Ln}^{3+}$  ions. In particular, bismuth-based fluoride nanoparticles have been proposed for multi-imaging and phosphor applications (Back et al., 2019), while bismuth oxyhalides of general formula  $\text{BiOX}$  ( $X = \text{F}, \text{Cl}, \text{Br}, \text{I}$ ) have been studied due to their chemical stability, high refractive index and photocatalytic properties (Wang et al., 2020b). Furthermore, bismuth-based compounds have been exploited in different fields such as luminescent thermometry (Back et al., 2020b; Casagrande et al., 2020), water splitting (Kato et al., 2017), fuel cells (Sanna et al., 2015), UV filtering (Zaccariello et al., 2019) and cosmetics production (Zaccariello et al., 2017). There are several synthetic routes to obtain sub-microparticles and nanoparticles of Bi-based systems with different shapes and morphology. One of these is the microwave-assisted synthesis, developed in the 80's (Gedye et al., 1986), that exploits microwave radiation with frequencies between 0.3 and 300 GHz as the heating source (Nüchter et al., 2004). As the microwave energy is not enough to break the chemical bonds, it increases the Brownian motion and consequently the temperature. During the reaction, the heat is

produced by the collisions of the particles, or by the electric dipole of molecules. Several advantages are ascribed to this synthetic method such as the high chemical yield, reproducibility and homogeneity of the synthesis, possible application in green chemistry, and contactless with the heating source (Dąbrowska et al., 2018). Therefore, sub-micro Bi-based fluoride and oxyfluoride particles can be easily synthesized through the microwave approach, with the possibility to obtain a high yield in powder (Escudero et al., 2014).

Here, we present the synthesis, structural and photophysical characterization of  $\text{Ln}^{3+}$ -doped ( $\text{Ln} = \text{Yb}, \text{Er}, \text{Tm}, \text{Eu}, \text{Tb}$ ) bismuth fluoride ( $\text{BiF}_3$ ) sub-micro particles prepared through a microwave-assisted synthesis, demonstrating that several  $\text{Ln}^{3+}$  ions can be efficiently hosted. The  $\text{Er}^{3+}$ - $\text{Yb}^{3+}$  co-doped sample was further explored for molecular logics and luminescent thermometry applications as it presents different emission profiles depending on the power density of the excitation laser. These results open a new path for all-photonic reprogrammable materials that are simultaneously primary thermometers, dismissing the need for recurrent thermal calibrations, and thus enabling the *in-situ* real-time monitoring of the temperature.

## Experimental details

### Chemical and materials

Bismuth nitrate pentahydrate ( $\text{Bi}(\text{NO}_3)_3 \cdot 5\text{H}_2\text{O}$ , Sigma  $\geq 99.99\%$ ), sodium tetrafluoroborate ( $\text{NaBF}_4$ , Across Organic,  $>97\%$ ) were used as bismuth and fluoride sources, respectively. Europium (III) nitrate pentahydrate ( $\text{Eu}(\text{NO}_3)_3 \cdot 5\text{H}_2\text{O}$ , Sigma Aldrich, 99.9%), terbium (III) nitrate pentahydrate ( $\text{Tb}(\text{NO}_3)_3 \cdot 5\text{H}_2\text{O}$ , Sigma Aldrich,  $\geq 99.9\%$ ), ytterbium (III) nitrate pentahydrate ( $\text{Yb}(\text{NO}_3)_3 \cdot 5\text{H}_2\text{O}$ , Sigma Aldrich,  $\geq 99.9\%$ ), erbium (III) nitrate pentahydrate ( $\text{Er}(\text{NO}_3)_3 \cdot 5\text{H}_2\text{O}$ , Sigma Aldrich,  $\geq 99.9\%$ ), thulium (III) nitrate pentahydrate ( $\text{Tm}(\text{NO}_3)_3 \cdot 5\text{H}_2\text{O}$ , Sigma Aldrich,  $\geq 99.9\%$ ), terbium (III) nitrate pentahydrate ( $\text{Tb}(\text{NO}_3)_3 \cdot 5\text{H}_2\text{O}$ , Sigma Aldrich,  $\geq 99.9\%$ ), holmium (III) nitrate pentahydrate ( $\text{Ho}(\text{NO}_3)_3 \cdot 5\text{H}_2\text{O}$ , Sigma Aldrich,  $\geq 99.9\%$ ) were used as  $\text{Ln}^{3+}$  precursors. Diethylene glycol (DEG, Sigma Aldrich,  $\geq 99.0\%$ ), and MilliQ water were used as solvents. Ethanol ( $\text{C}_2\text{H}_5\text{OH}$ , VWR Chemicals 100%) was used in the washing process.

### Synthesis of the sub-micro particles

The experimental protocol already reported elsewhere (Escudero et al., 2014) was adopted to produce oxyfluoride and fluoride bismuth materials. In short, pentahydrate bismuth nitrate,  $\text{Bi}(\text{NO}_3)_3 \cdot 5\text{H}_2\text{O}$ , is dissolved in 24 ml of

diethylene glycol at 348 K for 10 minutes under stirring and then the solution is cooled to room temperature. In the doping procedure,  $\text{Ln}^{3+}$  cations are dissolved in diethylene glycol together with the Bi precursor, with sodium tetrafluoroborate,  $\text{NaBF}_4$  in 6 ml of MilliQ water. These two solutions are then mixed under stirring and the resulting solution is placed in a Teflon-lined autoclave. The reaction occurs in a microwave digestion system (Ethos Plus Microwave, Milestone) at 393 K for 30 s, at 1000 W power. Afterward, the autoclave is quenched in an ice bath for 15 min. The opalescent solution obtained is separated by centrifugation (6,000 rpm) and the white precipitate is washed twice in ethanol and once in MilliQ water. The sample is dried overnight at room temperature and then characterized. The stoichiometry among reagents, temperature, and reaction time have been previously arranged to obtain octahedral sub-micro particles, as detailed in [Supplementary Table S1](#).

## Characterization

**Structural and morphological characterization:** X-ray powder diffraction (XRPD) measurements were performed on a diffractometer (Philips X'Pert) with a goniometer in the Bragg–Brentano geometry (PW 1319), connected to a highly stabilized X-ray source (Nickel-filtered  $\text{Cu-K}_\alpha$  radiation), a focusing graphite monochromator, and a proportional counter with a pulse height discriminator. A step-by-step technique with collection times of 10 s per step (steps of  $0.05^\circ$  in  $2\theta$  units) was employed.

The size, morphology, and EDX analysis of the sub-micro particles were carried out by a field emission scanning electron microscope (FE-SEM, Carl Zeiss Sigma VP) equipped with a microanalysis detector (Bruker Quantax 200). The EDX spectra were collected at 4–5 kV for all the samples. A second SEM equipment (JEOL JSM-5600LV) with a microanalysis system (OXFORD-Link Isis series 300) was used to perform the morphological analysis.

**Photoluminescence characterization:** The emission spectra of  $\text{BiF}_3:\text{Ln}^{3+}$  ( $\text{Ln} = \text{Eu}, \text{Tb}, \text{Yb}, \text{Er}$ ) were recorded with a modular double grating excitation spectrofluorometer with an emission monochromator (TRIAx 320, Fluorolog-3, Horiba Scientific) coupled to a photomultiplier (R928 Hamamatsu) operating in the visible spectral range, using a front face configuration. A 450 W Xe arc lamp was used as the excitation source for the  $\text{Eu}^{3+}$ - $\text{Tb}^{3+}$  single-doped and co-doped samples. Both recorded emission and excitation spectra were corrected with the spectrofluorimeter optical spectral response and the spectral distribution of the lamp intensity using a photodiode reference detector, respectively. For recording the temperature-dependent upconversion spectra of  $\text{BiF}_3:\text{Yb}^{3+}/\text{Er}^{3+}$  sample, a continuous-wave 980 nm laser diode (BrixX 980-1000 HD, Omicron Laser) focused through a NIR optical lens (Thorlabs, 12 cm focal distance) was used as the excitation

source. The temperature was controlled using a temperature controller (IES-RD31) equipped with a Kapton thermofoil heater (Minco) mounted on a Cu-holder. The temperature was recorded using a thermocouple (Barnant 100 model 600-2820) with an accuracy of 0.1 K, accordingly to the manufacturer.

The emission spectra of  $\text{Yb-Ln}^{3+}$  ( $\text{Ln} = \text{Tm}, \text{Ho}$ ) were acquired at Ca' Foscari University of Venice in the 250–1,050 nm range using a portable spectrometer (QE65 Pro, Ocean Optics), and a continuous-wave laser diode peaking at 980 nm (CNI MDL-III-980) as the excitation source. The laser diode output power was 2 W, distributed on a  $5 \times 8 \text{ mm}^2$  spot, corresponding to a mean power density of  $5 \text{ W cm}^{-2}$ .

## Luminescence thermometry

The temperature ( $T$ ) was accessed by the intensity ratio  $\Delta = I_H/I_S$ , where  $I_H$  and  $I_S$  the integrated areas of the  $\text{Er}^{3+}$  transitions  ${}^2\text{H}_{11/2} \rightarrow {}^4\text{I}_{15/2}$  and  ${}^4\text{S}_{3/2} \rightarrow {}^4\text{I}_{15/2}$ , respectively. The calculated temperature value is given by ([Balabhadra et al., 2017](#)):

$$\frac{1}{T} = \frac{1}{T_0} - \frac{k_B}{\Delta E} \ln \left( \frac{\Delta}{\Delta_0} \right) \quad (1)$$

where  $k_B$  is the Boltzmann constant,  $\Delta E$  is the energy gap between the barycenters of the  ${}^2\text{H}_{11/2} \rightarrow {}^4\text{I}_{15/2}$  and  ${}^4\text{S}_{3/2} \rightarrow {}^4\text{I}_{15/2}$  transitions,  $\Delta_0$  is the value of  $\Delta$  at the temperature  $T_0$  in the limit of null excitation power density. The performance of luminescent thermometers is quantified by the relative thermal sensitivity ( $S_r$ ) and temperature uncertainty ( $\delta T$ ). According to the corresponding definitions ([Brites et al., 2017](#)):

$$S_r = \frac{1}{\Delta} \left| \frac{\partial \Delta}{\partial T} \right| = \frac{\Delta E}{k_B T^2} \quad (2)$$

and

$$\delta T = \frac{1}{S_r} \frac{\delta \Delta}{\Delta} = \frac{k_B T^2}{\Delta E} \frac{\delta \Delta}{\Delta} \quad (3)$$

where  $\delta \Delta / \Delta$  is the relative uncertainty in  $\Delta$  estimated here for each temperature using the signal to noise ratio of the corresponding recorded emission spectrum.

## Results and discussion

### Synthesis, structure and morphology of the $\text{Ln}^{3+}$ -doped $\text{BiF}_3$ particles

The mechanism of formation of the sub-micro particles is not fully understood since the microwave-assisted reaction takes place very quickly ([Escudero et al., 2014](#)). [Figures 1A–F](#) shows the surface morphology of  $\text{BiF}_3$  sub-micro particles  $\text{Ln}^{3+}$ -doped and undoped obtained by microwave synthesis. It is assumed that spheres are initially formed which then evolve into octahedral

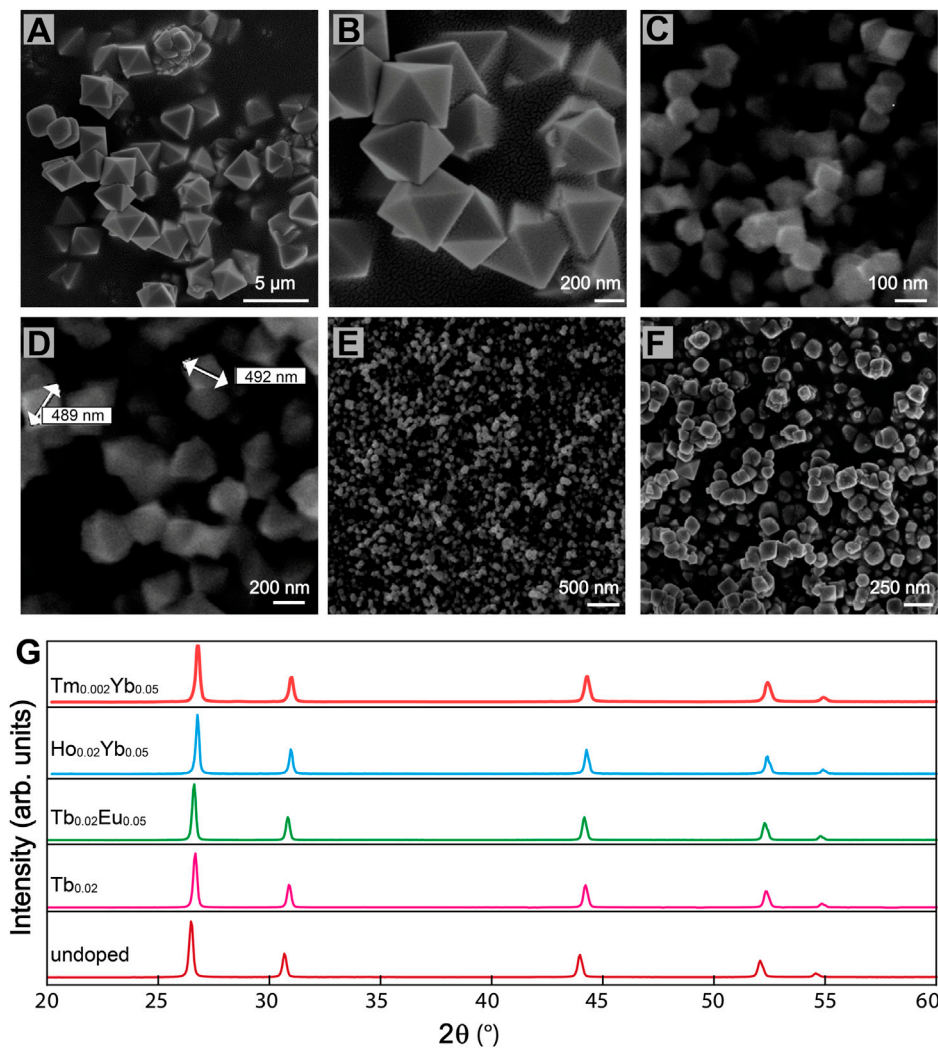


**FIGURE 1**  
SEM micrographs of BiF<sub>3</sub> sub-micro particles (A) (B) Eu<sub>0.05</sub> doped, (C) (D) undoped, (E) Er<sub>0.02</sub> doped, (F) Er<sub>0.01</sub>Yb<sub>0.05</sub> co-doped. (G) XRD patterns of BiF<sub>3</sub> sample undoped and Ln<sup>3+</sup> single and co-doped.

shapes (Figures 1A–D), with an average size between 300 and 600 nm (Supplementary Figures S1A,B). As reported in the literature (Escudero et al., 2014), octahedral sub-micro particles are formed in a short time (30 s) as soon as the temperature reaches the set maximum (393 K). Smaller dimensions could be obtained using different molar ratios among reagents. For example, using a higher NaBF<sub>4</sub> concentration (Supplementary Table S1), resulted in a smaller size, around 130–150 nm (Supplementary Figure S2A). The decrease in the average size of the octahedral sub-micro particles is probably due to the largest number of nuclei involved during the reaction process.

On one hand, for samples with a low concentration of dopants octahedral is the predominant shape (Figure 1E), on the other hand, with a higher concentration of dopants, the

micrographs revealed agglomerated granules (Figure 1F). We observed that when the amount of Ln<sup>3+</sup> ions is higher than 5.0 atomic %, the thermodynamic equilibrium is altered and particles with different shapes are obtained (Supplementary Figure S2B).

Figure 1G suggests all the synthesized samples exhibit the same XRD pattern, attributable to α-BiF<sub>3</sub> cubic structure (ICSD#2452 card). The adopted microwave-assisted synthesis route can determine the incorporation of the oxygen into the α-BiF<sub>3</sub> structure that leads to the formation of BiO<sub>y</sub>F<sub>3–2y</sub> solid solutions (Escudero et al., 2014), and thus, diverse solid solutions based on the cubic fluorite, orthorhombic, monoclinic, rhombohedral, and hexagonal structures have been reported so far (Bervas et al., 2006).

The elemental mapping energy performed through X-ray (EDX) confirms the homogeneous distribution of elements in the

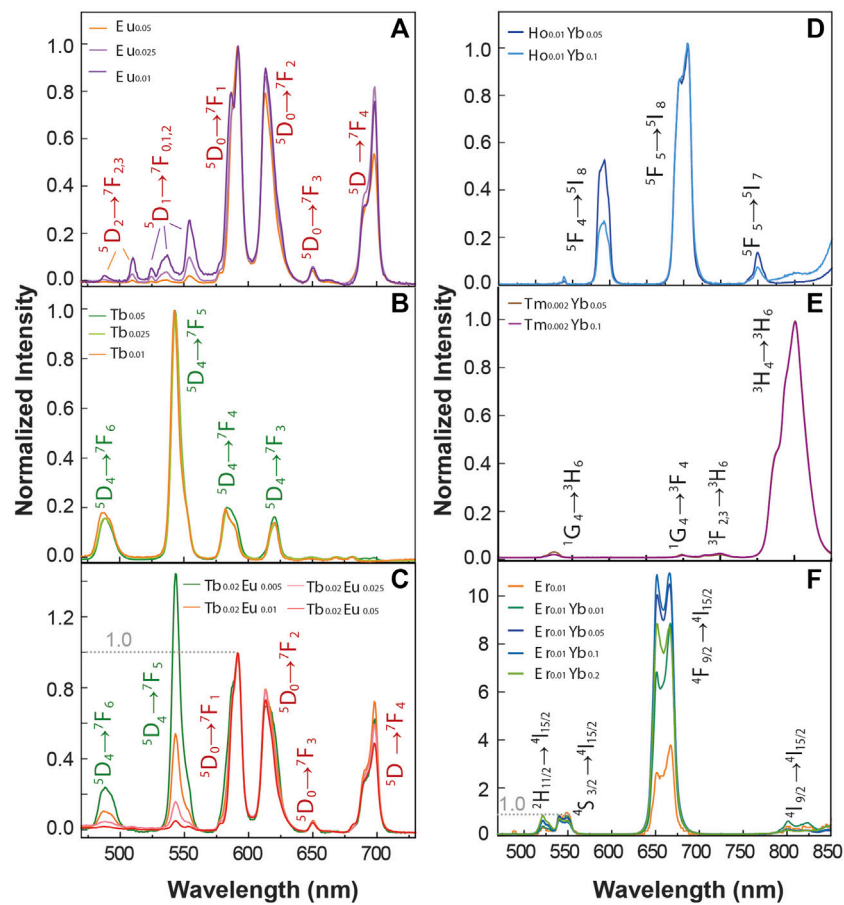


FIGURE 2

Emission spectra of (A)  $\text{Eu}^{3+}$  single-doped (B)  $\text{Tb}^{3+}$  single-doped, and (C)  $\text{Tb}^{3+}$ - $\text{Eu}^{3+}$  co-doped samples under 370 nm excitation. The transitions assigned the  $\text{Tb}^{3+}$  and  $\text{Eu}^{3+}$  ions are presented in green and red colors, respectively. Upconversion emission spectra of (D)  $\text{Yb}^{3+}$   $\text{Tm}^{3+}$  co-doped, (E)  $\text{Yb}^{3+}$   $\text{Ho}^{3+}$  co-doped and (F)  $\text{Yb}^{3+}$   $\text{Er}^{3+}$  co-doped and single doped  $\text{Er}^{3+}$  samples upon 980 nm excitation.

$\text{Ln}^{3+}$  doped particles. The elemental mapping of  $\text{BiF}_3$  confirmed that all the elements were finely dispersed over the entire analyzed area (Supplementary Figure S4).

## Photoluminescence characterization

It is widely known that the luminescence intensity of  $\text{Ln}^{3+}$  ions is sensitive to the concentration of the dopants. Looking forward to studying the optical properties of the material, we synthesized  $\text{BiF}_3$  particles incorporating different concentrations of  $\text{Ln}^{3+}$  ions. Figure 2 displays a series of  $\text{Ln}^{3+}$  single-doped and co-doped samples. Figures 2A–C shows the emission spectra for  $\text{Eu}^{3+}$  and  $\text{Tb}^{3+}$  single-doped and co-doped samples under 370 nm excitation. The narrow lines (FWHM <10 nm) are ascribed to the  $\text{Tb}^{3+}$  ( $^5\text{D}_4 \rightarrow ^7\text{F}_{3-6}$ ) and  $\text{Eu}^{3+}$  ( $^5\text{D}_0 \rightarrow ^7\text{F}_{0-4}$ ) transitions. The  $\text{Tb}^{3+}$  single-doped samples are normalized to the peak intensity of

$^5\text{D}_4 \rightarrow ^7\text{F}_4$  transition for comparison. The  $\text{Eu}^{3+}$  single-doped and  $\text{Tb}^{3+}$  co-doped samples instead are normalized to the peak intensity of  $^5\text{D}_0 \rightarrow ^7\text{F}_1$  transition. From the  $\text{Eu}^{3+}$  samples, the relative intensity of the  $^5\text{D}_1 \rightarrow ^7\text{F}_{0,3}$  and  $^5\text{D}_0 \rightarrow ^7\text{F}_{1,2}$  decreases as the  $\text{Eu}^{3+}$  concentration increases. One important transition is the  $\text{Eu}^{3+}$   $^5\text{D}_0 \rightarrow ^7\text{F}_1$  one (centered at 591 nm), a magnetic dipole transition (MD), allowed by the selection rules. The  $^5\text{D}_0 \rightarrow ^7\text{F}_1$  transition is usually less intense than the  $^5\text{D}_0 \rightarrow ^7\text{F}_2$  one (Binnemans, 2015). For the  $\text{BiF}_3$  host, however, the MD transition is most intense due to the  $\text{Eu}^{3+}$  cations occupying crystallographic sites with an inversion center, which is compatible with the replacement of  $\text{Bi}^{3+}$  by  $\text{Eu}^{3+}$  cations (Escudero et al., 2014). Moreover, emission bands originating from the  $^5\text{D}_1$  emitting level are clearly observed at low temperatures for the sample doped with a  $\text{Eu}^{3+}$  concentration of 5 mol% due to the suppression of non-radiative processes responsible for the thermal quenching at room temperature. We

stress the presence of  $^5D_1 \rightarrow ^7F_0$  transition that usually is not allowed for  $\text{Eu}^{3+}$  in centrosymmetric sites, in line with previous reports in other matrices with similar local symmetry (Tanner, 2013). The above-described  $\text{Eu}^{3+}$  transitions are usually observed in matrices with very low phonon energy, that are very convenient as hosts. In the  $\text{Eu}^{3+}/\text{Tb}^{3+}$  co-doped samples, there is evidence of a  $\text{Tb}^{3+}$ -to- $\text{Eu}^{3+}$  energy transfer as signed by the intra- $4f^8$  transitions lines observed in the  $\text{Eu}^{3+}$  excitation spectra (Supplementary Figure S5A), together with the decrease of the emission intensity for the  $\text{Tb}^{3+}$  transitions as the  $\text{Eu}^{3+}$  concentration increases (Figure 2C).

Figures 2D–F shows the upconversion emission spectra of a series of  $\text{Ln}^{3+}$  single-doped and  $\text{Yb}^{3+}$ - $\text{Ln}^{3+}$  ( $\text{Er}^{3+}$ ,  $\text{Tm}^{3+}$ ,  $\text{Ho}^{3+}$ ) co-doped samples upon 980 nm excitation. The emission  $\text{Ho}^{3+}/\text{Yb}^{3+}$  co-doped samples (Figure 2D) show the emissions bands of  $\text{Ho}^{3+}$  ions in the green, red, and near-infrared spectral ranges, originating from the  $^5F_4 \rightarrow ^5I_8$  (~540 nm),  $^5F_5 \rightarrow ^5I_8$  (~650 nm), and  $^5F_4 \rightarrow ^5I_7$  (~750 nm) transitions, respectively. The emission spectra recorded for the  $\text{Tm}^{3+}/\text{Yb}^{3+}$  co-doped samples are presented in Figure 2E, and the peaks ascribed to the  $\text{Tm}^{3+}$  transitions  $^1G_4 \rightarrow ^3H_6$  at 475 nm,  $^1G_4 \rightarrow ^3F_4$  (~650 nm),  $^3F_2,3 \rightarrow ^3H_6$  (~700 nm) and  $^3H_4 \rightarrow ^3H_6$  (~795 nm) are observed. Figure 2F presents the emission spectra of the  $\text{Er}^{3+}/\text{Yb}^{3+}$  co-doped samples, in which the emission bands ascribed to  $^2H_{11/2} \rightarrow ^4I_{15/2}$  (~520 nm),  $^4S_{3/2} \rightarrow ^4I_{15/2}$  (~550 nm) and  $^4F_{9/2} \rightarrow ^4I_{15/2}$  (~650 nm) transitions are observed. In all the  $\text{Yb}^{3+}$ - $\text{Ln}^{3+}$  samples, the recorded upconverting emission involves the  $\text{Yb}^{3+}$   $^2F_{5/2}$  level population by ground state absorption, followed by  $\text{Yb}^{3+}$ -to-acceptor energy transfer mechanisms (Dong et al., 2015). The acceptor ions ( $\text{Ho}^{3+}$ ,  $\text{Tm}^{3+}$ ,  $\text{Er}^{3+}$ ) are first promoted to their respective excited states and then relax originating the observed spectral features. The energy diagram illustrating a possible route for the energy transfer processes is depicted in Supplementary Figure S6.

## Exploiting $\text{BiF}_3$ : $\text{Yb}^{3+}/\text{Er}^{3+}$ particles for primary thermometry

Primary thermometers are temperature sensors in which the temperature determination is based on well-grounded physical principles. In 2017, Balabhadra et al. (2017) proposed a straightforward method to predict the temperature calibration curve of any upconverting thermometer based on two thermally coupled electronic levels using the Boltzmann statistics. Here, we selected an  $\text{Er}^{3+}/\text{Yb}^{3+}$  co-doped sample (1% of Er and 5% of Yb) hereafter denominated  $\text{BiF}_3$ : $\text{YbEr}$ . Figure 3A displays the temperature-dependent upconversion emission spectra of  $\text{BiF}_3$ : $\text{YbEr}$  recorded under 980 nm excitation between 298 and 363 K. Figure 3B shows the thermal dependence of the integrated areas of the  $\text{Er}^{3+}$  transitions  $^2H_{11/2} \rightarrow ^4I_{15/2}$  and  $^4S_{3/2} \rightarrow ^4I_{15/2}$  and corresponding to the  $I_H$  (510–533 nm) and  $I_S$  (533–570 nm),

respectively. We observe two regimes, depending on the temperature range: for  $T < 320$  K the  $I_H$  transition remains constant, and  $I_S$  decreases about 25%, whereas for higher temperatures both  $I_H$  and  $I_S$  increase. The parameter that allows the conversion of the integrated areas into temperature is the so-called thermometric parameter, defined as  $\Delta = I_H/I_S$  (Figure 3C).

According to the established methodology (S. Balabhadra et al., 2017), the calibration curve can be predicted if the energy separation between the emitting levels ( $\Delta E$ ) and the  $\Delta$  value in the limit of null excitation power density,  $\Delta_0$  (at temperature  $T_0$ , calculus in Supporting Information) can be obtained independently. The  $\Delta E$  value is calculated by the difference between the barycenter of the emission spectra recorded at room temperature, resulting  $\Delta E = 768 \pm 25 \text{ cm}^{-1}$  (calculus in Supporting Information). This value agrees with that reported for  $\text{Yb}^{3+}/\text{Er}^{3+}$  co-doped systems (Hernández-Rodríguez et al., 2021). The  $\Delta_0$  value, estimated at room temperature ( $T_0 = 298.0 \pm 0.1$  K) as the extrapolation for null excitation power densities of the thermometric parameter, is  $\Delta_0 = 0.16 \pm 0.01$ .

The maximum  $S_r$  value was observed for the lower temperature value tested (298 K) of  $1.3 \pm 0.1\% \text{ K}^{-1}$  and the minimum  $\delta T = 0.4$  K was estimated at the same temperature (Figure 3E,F). As the temperature increases,  $S_r$  decreases reaching  $0.9 \pm 0.1\% \text{ K}^{-1}$  at 365 K. The corresponding thermal uncertainty increases to 0.7 K. We conclude that  $\text{BiF}_3$ : $\text{YbEr}$  sub-micro particles exhibited comparable  $S_r$  values to those reported for optical thermometers based on  $\text{Yb}^{3+}/\text{Er}^{3+}$  (Table 1) as expected since the  $\Delta E$  value obtained here (that is determining the maximum  $S_r$ ), is comparable to that found in the literature (Hernández-Rodríguez et al., 2021). The validity of Eq. 1 to predict the temperature was verified in the range 295–365 K. Figure 3D presents a comparison between measured (by a thermocouple, uncertainty of 0.1 K) and calculated temperature values in that temperature range. There is a perfect match between calculated and measured temperature values within the uncertainty of both quantities, thus attesting that the studied system is a primary thermometer with temperature determined via Eq. 1. These results sustain that  $\text{BiF}_3$ : $\text{YbEr}$  sub-micro particles are primary luminescent thermometers working in a wide range of temperatures.

## Exploiting $\text{BiF}_3$ : $\text{Yb}^{3+}/\text{Er}^{3+}$ particles for molecular logic

The  $\text{BiF}_3$ : $\text{YbEr}$  particles present emission features that are dependent on the temperature and on the excitation power density employed. Rationalizing these observations in the context of molecular logic, we exploit external stimuli (e.g., excitation power density,  $P_D$ , and  $T$ ) and several logic outputs, considering the modifications induced in the emission spectra (Figures 4A,B). First, we calculate the intensity of some Stark

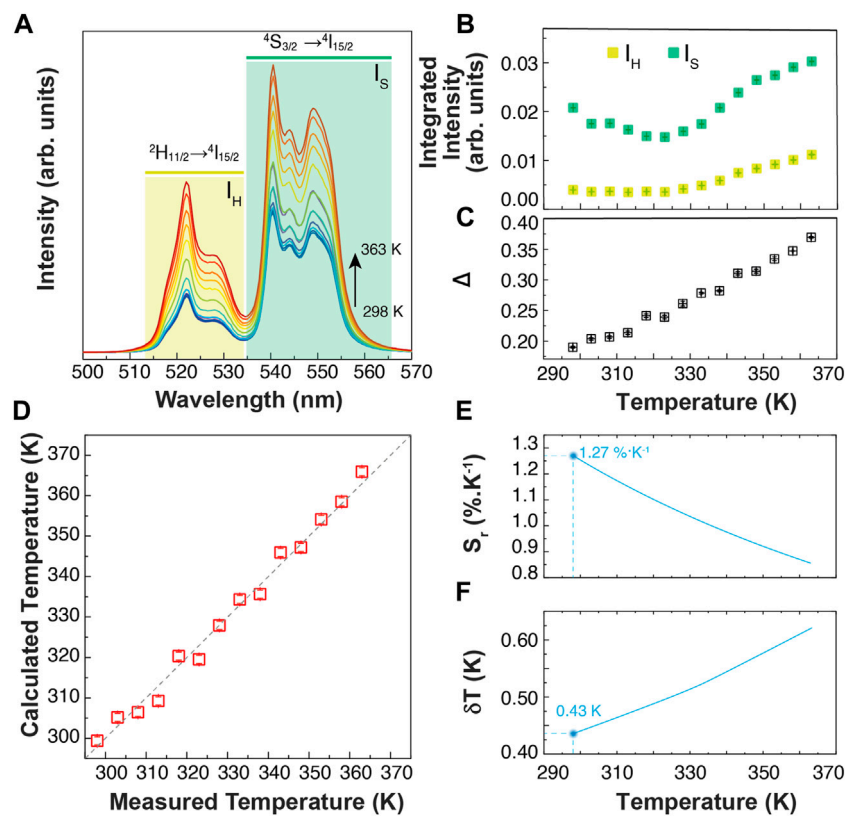


FIGURE 3

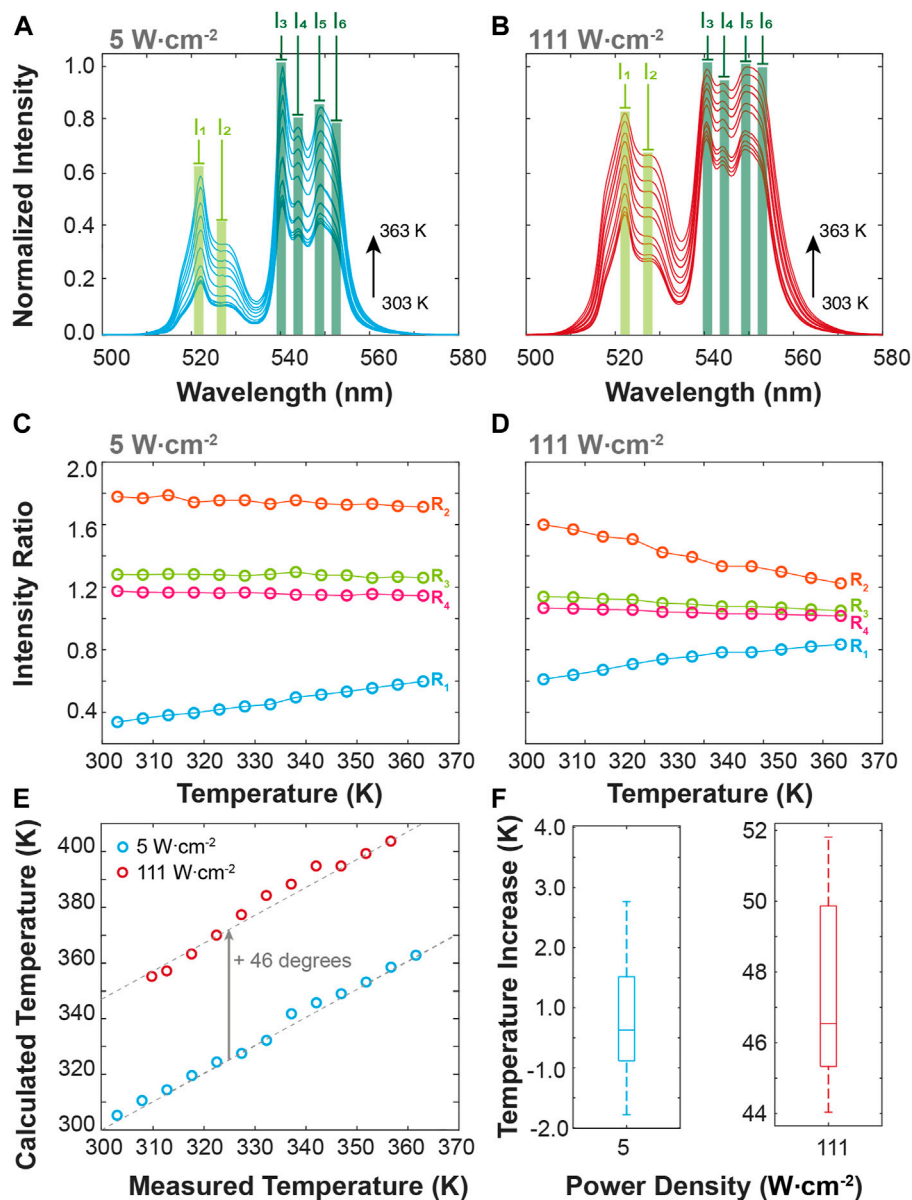
(A) Temperature-dependent upconversion emission spectra of BiF<sub>3</sub>:YbEr upon 980 nm excitation ( $P_D = 5 \text{ W cm}^{-2}$ ). The shadowed areas correspond to the integration ranges. (B) Temperature dependence of the emission band integrated areas related to the  ${}^2\text{H}_{11/2} \rightarrow {}^4\text{I}_{15/2}$  ( $I_H$ ) and  ${}^4\text{S}_{3/2} \rightarrow {}^4\text{I}_{15/2}$  ( $I_S$ ) Er<sup>3+</sup> transitions. The corresponding calibration curve is presented in (C). (D) Comparison between the measured ( $x$ -axis) and the calculated through Eq. 1 ( $y$ -axis) temperatures. The interrupted line is a guide to the eyes corresponding to  $y = x$ . (E) Relative thermal sensitivity and (F) temperature uncertainty of BiF<sub>3</sub>:YbEr expressed as  $S_r$ , obtained through Eq. 2 and Eq. 3, respectively.

TABLE 1 Working temperature range, excitation wavelength ( $\lambda_x$ , nm), relative sensitivity ( $S_r$ , %K<sup>-1</sup>) and corresponding temperature value ( $T$ ) for which it is reported of illustrative Ln<sup>3+</sup>- based optical temperature sensors involving the ratio of the emission integrated areas of the Er<sup>3+</sup> transitions.

Compounds	Temperature range (K)	$\lambda_x$ (nm)	$S_r$ (%K <sup>-1</sup> )	$T$ (K)	Ref
NaYF <sub>4</sub> :Er <sup>3+</sup> /Yb <sup>3+</sup>	300–773	980	1.2	300	Li et al. (2019)
Ca <sub>3</sub> Al <sub>2</sub> O <sub>6</sub> :Er <sup>3+</sup> /Yb <sup>3+</sup>	298–573	980	0.8	145	Wang et al. (2019)
BiOF:Er <sup>3+</sup>	303–663	980	1.1	303	Wang et al. (2020a)
Bi <sub>2</sub> SiO <sub>5</sub> :Yb,Er@SiO <sub>2</sub>	80–800	980	1.1	300	Back et al. (2020a)
SrS:Ce <sup>3+</sup> /Er <sup>3+</sup>	100–300	410	0.3	100	Wei et al. (2022)
BiF <sub>3</sub> :ErYb	298–365	980	1.3	298	This work

components of the Er<sup>3+</sup> transitions  ${}^4\text{S}_{3/2}$ ,  ${}^2\text{H}_{11/2} \rightarrow {}^4\text{I}_{15/2}$  transition, selecting the peak wavelengths, namely the 522.0 ( $I_1$ ) and 527.0 nm ( $I_2$ ) wavelengths, in the  ${}^4\text{S}_{3/2} \rightarrow {}^4\text{I}_{15/2}$  transition, and the 540.5, 544.0, 549.0 and 552 nm wavelengths ( $I_3$  to  $I_6$ , respectively) in the  ${}^2\text{H}_{11/2} \rightarrow {}^4\text{I}_{15/2}$  one. These intensities allow us to define four ratiometric outputs, as  $R_1 = I_1/I_3$ ;  $R_2 = I_1/I_2$ ;  $R_3 =$

$I_3/I_4$ , and  $R_4 = I_5/I_6$ . The ratiometric definition of the logic outputs guarantees that the system is independent of eventual fluctuations in the excitation source intensity and/or electrical drifts of the detection system. The temperature dependence of the intensity ratios is presented in Figures 4C,D for low (5 W·cm<sup>-2</sup>) and high (111 W cm<sup>-2</sup>)  $P_D$  values. As the particles



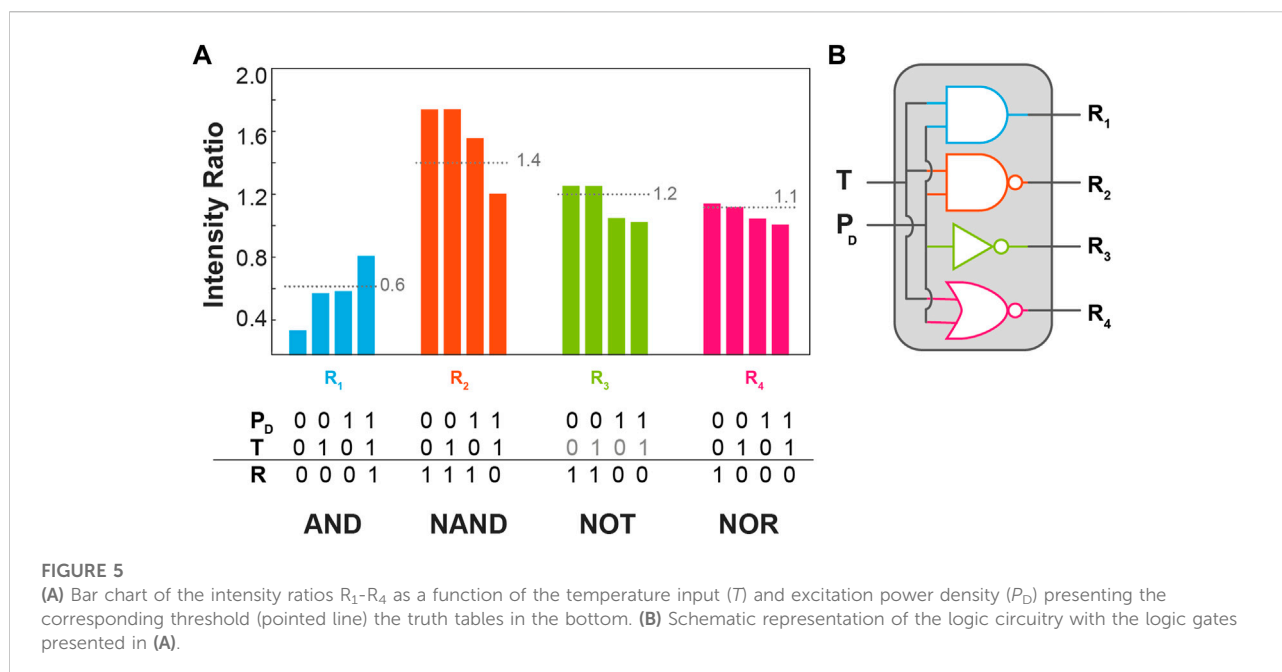
**FIGURE 4**

Temperature-dependent upconversion emission spectra of  $\text{BiF}_3:\text{YbEr}$  upon 980 nm excitation at (A) 5 and (B) 111  $\text{W cm}^{-2}$ . (C) Intensities ratio as a function of the temperature calculated from the emission spectra at (C) 5 and (D) 111.1  $\text{W cm}^{-2}$ . (E) Comparison between the measured (set in the temperature controller) and the calculated (Eq. 1) temperature values for the 5 and 111  $\text{W cm}^{-2}$ . The interrupted lines are guides to the eyes corresponding to  $y = x$  (overlapping the blue symbols) and  $y = x + 46.3$  (overlapping the red symbols). The corresponding boxplots of the temperature increase are presented in (F).

are luminescent primary thermometers, we can determine the actual local temperature upon 980 nm irradiation. The comparison between the measured temperature (set in the temperature controller) and that calculated using Eq. 1 is presented in Figure 4E. As expected, the increase of the  $P_D$  value induces local heating on the particles independent of the temperature set in the controller, reaching a median value of  $0.3^\circ$  for  $5 \text{ W cm}^{-2}$  (comparable to the temperature uncertainty of the

thermometer) and  $43.3^\circ\text{C}$  for  $111 \text{ W cm}^{-2}$  (Figure 4F). These values are comparable to those reported by Bhiri *et al.* using  $\text{GdVO}_4:\text{Yb}^{3+}/\text{Er}^{3+}$  microcrystals [ $\sim 50^\circ\text{C}$  at  $100 \text{ W cm}^{-2}$ , (Bhiri *et al.*, 2022)].

To demonstrate the application of the  $\text{BiF}_3:\text{YbEr}$  particles to molecular logic we represent the dependence of the intensity ratios defined above ( $R_1$ - $R_4$ ) on the temperature and the excitation power density, Figure 5A. The excitation



radiation was not employed as a logic input being an *a priori* condition for the activation of the logic gate. The logic inputs are digitalized to 0 and 1 using the room temperature (305 K) set in the temperature controller as 0 and 360 K as 1. For  $P_D$  the logic input 0 was set to  $5 \text{ W cm}^{-2}$  and the logical value 1–111  $\text{W cm}^{-2}$ . For each intensity ratio, a threshold value (pointed lines in Figure 5A) was arbitrarily set to get the higher number of distinct logic gates as possible. The corresponding truth tables were then constructed setting the logical values of 1 for the intensity ratios above the thresholds. The ratios  $R_1$ ,  $R_2$ , and  $R_4$  correspond to AND, NAND, and NOR logic gates whereas the ratio  $R_3$  is insensitive to the temperature, yielding simply a NOT gate on the logic input  $P_D$ . This is the first time the same upconversion emission is used to define multiple logic gates, constituting an equivalent molecular chipset as represented in Figure 5B.

## Conclusion

$\text{BiF}_3:\text{Ln}^{3+}$  ( $\text{Ln} = \text{Yb}, \text{Er}, \text{Tm}, \text{Eu}, \text{Tb}$ ) sub-micro particles were successfully prepared via microwave-assisted synthesis. Monodispersed octahedra sub-micro particles were obtained with  $\text{Ln}^{3+}$  doping concentration <5 atomic %, while at higher concentrations of dopants the shape is no longer octahedral and spheres and aggregated are predominant. The crystalline structure of the materials is not altered by the concentration of the dopants. Through a microwave synthesis approach, we obtained samples with high reproducibility and the

possibility of a vast field of applications, even on the industrial scale.

All the prepared  $\text{BiF}_3:\text{Ln}^{3+}$  sub-micro particles display a detectable emission, both for downshifting and upconverting emission. We conclude that  $\text{Ln}^{3+}$ -doped  $\text{BiF}_3$  sub-micro particles synthesized through the microwave-assisted method are suitable for observing downshifting and upconversion emissions. The matrix has an important role due to the intrinsic low phonon energy that strongly determines the balance between the probabilities of radiative and non-radiative processes such as multiphonon relaxation and cross-relaxation mechanisms. The intrinsic low phonon energy of the  $\text{BiF}_3$  host is an advantage that allows us to observe transitions that are obscured in other fluoride host matrixes such as  $\text{NaYF}_4$ .

We characterized  $\text{Er}^{3+}\text{-Yb}^{3+}$  co-doped  $\text{BiF}_3$  particles under 980 nm excitation for luminescence thermometry and molecular logic. We proved that these particles are luminescent primary thermometers with relative sensitivity up to  $1.27\% \text{ K}^{-1}$  and temperature uncertainty down to 0.4 K, values in good agreement with those in the literature for  $\text{Yb}^{3+}/\text{Er}^{3+}$  co-doped upconverting nanoparticles. Moreover, this sample presents emission features that are dependent on the excitation power density and the temperature, and thus, as an illustrative example, we defined a molecular chipset constituted of four independent logic gates (AND, NAND, NOR, and NOT) by analyzing the  ${}^2\text{H}_{11/2} \rightarrow {}^4\text{I}_{15/2}$  and  ${}^4\text{S}_{3/2} \rightarrow {}^4\text{I}_{15/2}$   $\text{Er}^{3+}$  transitions. The next challenge will be to employ these particles to define more complex operations involving more emitting centers and diverse external stimuli, looking forward to yielding logical reconfiguration, thus demonstrating that bismuth-based

materials are suitable for molecular computing in all-photonics logical devices.

## Data availability statement

The original contributions presented in the study are included in the article/Supplementary Materials, further inquiries can be directed to the corresponding author.

## Author contributions

SZ: Original draft and original figures preparation, synthesis of the particles, and photophysical characterization. ET, EM, AT, MB: Conceptualization, supervising the synthesis of the particles, data curation, and validation of the synthesis and structural characterization of the prepared particles. LC, RF, CB: Conceptualization of the luminescent thermometry and molecular logic experiments, methodology on photoluminescence measurements, data curation on photoluminescence for luminescent thermometry and molecular logic, software, validation, writing, reviewing, and editing on the final manuscript and figures.

## Funding

This work was developed within the scope of the project CICECO-Aveiro Institute of Materials, UIDB/50011/2020, UIDP/50011/2020 & LA/P/0006/2020, financed by national

## References

- Alivisatos, A. P. (1996). Semiconductor clusters, nanocrystals, and quantum dots. *Science* 271, 933–937. doi:10.1126/science.271.5251.933
- Andréasson, J., and Pischel, U. (2021). Light-stimulated molecular and supramolecular systems for information processing and beyond. *Coord. Chem. Rev.* 429, 213695. doi:10.1016/j.ccr.2020.213695
- Andréasson, J., Pischel, U., Straight, S. D., Moore, T. A., Moore, A. L., and Gust, D. (2011). All-photonics multifunctional molecular logic device. *J. Am. Chem. Soc.* 133, 11641–11648. doi:10.1021/ja203456h
- Back, M., Casagrande, E., Brondin, C. A., Ambrosi, E., Cristofori, D., Ueda, J., et al. (2020a). Lanthanide-doped Bi<sub>2</sub>SiO<sub>5</sub>@SiO<sub>2</sub> core-shell upconverting nanoparticles for stable ratiometric optical thermometry. *ACS Appl. Nano Mater.* 3, 2594–2604. doi:10.1021/acsnm.0c00003
- Back, M., Casagrande, E., Trave, E., Cristofori, D., Ambrosi, E., Dallo, F., et al. (2020b). Confined-melting-assisted synthesis of bismuth silicate glass-ceramic nanoparticles: Formation and optical thermometry investigation. *ACS Appl. Mater. Interfaces* 12, 55195–55204. doi:10.1021/acsmi.0c17897
- Back, M., Ueda, J., Ambrosi, E., Cassandro, L., Cristofori, D., Ottini, R., et al. (2019). Lanthanide-doped bismuth-based fluoride nanocrystalline particles: Formation, spectroscopic investigation, and chemical stability. *Chem. Mat.* 31, 8504–8514. doi:10.1021/acs.chemmater.9b03164
- Bai, X., Caputo, G., Hao, Z. D., Freitas, V. T., Zhang, J. H., Longo, R. L., et al. (2014). Efficient and tuneable photoluminescent boehmite hybrid nanoplates lacking metal activator centres for single-phase white LEDs. *Nat. Commun.* 5, 5702. doi:10.1038/ncomms6702
- Balabhadra, S., Debasu, M. L., Brites, C. D. S., Ferreira, R. A. S., and Carlos, L. D. (2017). Upconverting nanoparticles working as primary thermometers in different media. *J. Phys. Chem. C* 121, 13962–13968. doi:10.1021/acs.jpcc.7b04827
- Bervas, M., Yakshinskiy, B., Klein, L. C., and Amatucci, G. G. (2006). Soft-chemistry synthesis and characterization of bismuth oxyfluorides and ammonium bismuth fluorides. *J. Am. Ceram. Soc.* 89, 645–651. doi:10.1111/j.1551-2916.2005.00721.x
- Bhiri, N. M., Dammak, M., Carvajal, J. J., Aguiló, M., Díaz, F., and Pujol, M. C. (2022). Excitation power density dependence of a primary luminescent thermometer based on Er<sup>3+</sup>, Yb<sup>3+</sup>: GdVO<sub>4</sub> microcrystals operating in the visible. *J. Alloys Compd.* 921, 166020. doi:10.1016/j.jallcom.2022.166020
- Binnemans, K. (2015). Interpretation of europium(III) spectra. *Coord. Chem. Rev.* 295, 1–45. doi:10.1016/j.ccr.2015.02.015
- Brites, C. D. S., Balabhadra, S., and Carlos, L. D. (2019). Lanthanide-based thermometers: At the cutting-edge of luminescence thermometry. *Adv. Opt. Mater.* 7, 1801239. doi:10.1002/adom.201801239
- Brites, C. D. S., Millán, A., and Carlos, L. D. (2017). “Lanthanides in luminescent thermometry,” in *Handbook on the Physics and Chemistry of Rare Earths*. Editors J.-C. G. Bünzli and V. K. Pecharsky (Amsterdam: Elsevier Science).
- Bünzli, J.-C. G. (2015). On the design of highly luminescent lanthanide complexes. *Coord. Chem. Rev.* 293, 19–47. doi:10.1016/j.ccr.2014.10.013
- Casagrande, E., Back, M., Cristofori, D., Ueda, J., Tanabe, S., Palazzolo, S., et al. (2020). Upconversion-mediated Boltzmann thermometry in double-layered Bi

funds through the FCT/MEC (PIDDAC). Financial support from the project LogicALL (PTDC/CTM-CTM/0298/2020) Portuguese funds through FCT/MCTES, is acknowledged. SZ acknowledges Fundação da Ciência e Tecnologia (Portugal) for a Ph.D. grant (SFRH/BD/144239/2019) financed by Portuguese national funds through the FCT/MEC and when appropriate co-financed by FEDER.

## Conflict of interest

The authors declare that the research was conducted in the absence of any commercial or financial relationships that could be construed as a potential conflict of interest.

## Publisher's note

All claims expressed in this article are solely those of the authors and do not necessarily represent those of their affiliated organizations, or those of the publisher, the editors and the reviewers. Any product that may be evaluated in this article, or claim that may be made by its manufacturer, is not guaranteed or endorsed by the publisher.

## Supplementary material

The Supplementary Material for this article can be found online at: <https://www.frontiersin.org/articles/10.3389/fphot.2022.1010958/full#supplementary-material>

- 2 SiO<sub>5</sub>:Yb<sup>3+</sup>, Tm<sup>3+</sup>@ SiO<sub>2</sub> hollow nanoparticles. *J. Mat. Chem. C* 8, 7828–7836. doi:10.1039/d0tc01457e
- Chen, G., Yang, C., and Prasad, P. N. (2013). Nanophotonics and nanochemistry: Controlling the excitation dynamics for frequency up-and down-conversion in lanthanide-doped nanoparticles. *Acc. Chem. Res.* 46, 1474–1486. doi:10.1021/ar300270y
- Dałbrowska, S., Chudoba, T., Wojnarowicz, J., and Łojkowski, W. (2018). Current trends in the development of microwave reactors for the synthesis of nanomaterials in laboratories and industries: A review. *Crystals* 8, 379. doi:10.3390/cryst8100379
- De Silva, A. P., Gunaratne, N. H. Q., and McCoy, C. P. (1993). A molecular photoionic AND gate based on fluorescent signalling. *Nature* 364, 42–44. doi:10.1038/364042a0
- Deng, R., Qin, F., Chen, R., Huang, W., Hong, M., and Liu, X. (2015). Temporal full-colour tuning through non-steady-state upconversion. *Nat. Nanotechnol.* 10, 237–242. doi:10.1038/nnano.2014.317
- Dong, H., Sun, L.-D., and Yan, C.-H. (2015). Energy transfer in lanthanide upconversion studies for extended optical applications. *Chem. Soc. Rev.* 44, 1608–1634. doi:10.1039/c4cs00188e
- Erbaş-Cakmak, S., Kolemen, S., Sedgwick, A. C., Gunnlaugsson, T., James, T. D., Yoon, J., et al. (2018). Molecular logic gates: The past, present and future. *Chem. Soc. Rev.* 47, 2228–2248. doi:10.1039/c7cs00491e
- Escudero, A., Moretti, E., and Ocaña, M. (2014). Synthesis and luminescence of uniform europium-doped bismuth fluoride and bismuth oxyfluoride particles with different morphologies. *CrystEngComm* 16, 3274. doi:10.1039/c3ce42462f
- Gedye, R., Smith, F., Westaway, K., Ali, H., Baldisera, L., Laberge, L., et al. (1986). The use of microwave ovens for rapid organic synthesis. *Tetrahedron Lett.* 27, 279–282. doi:10.1016/s0040-4039(00)83996-9
- Hernández-Rodríguez, M. A., Kamada, K., Yoshikawa, A., Muñoz-Santiuste, J. E., Casanovas-Melián, A., Martín, I. R., et al. (2021). 1000 K optical ratiometric thermometer based on Er<sup>3+</sup> luminescence in yttrium gallium garnet. *J. Alloys Compd.* 886, 161188. doi:10.1016/j.jallcom.2021.161188
- Jaque, D., and Vetrone, V. (2012). Luminescence nanothermometry. *Nanoscale* 4, 4301. doi:10.1039/c2nr30764b
- Kato, D., Hongo, K., Maezono, R., Higashi, M., Kunioku, H., Yabuuchi, M., et al. (2017). Valence band engineering of layered bismuth oxyhalides toward stable visible-light water splitting: Madelung site potential analysis. *J. Am. Chem. Soc.* 139, 18725–18731. doi:10.1021/jacs.7b11497
- Kumar, D., Sharma, S. K., Verma, S., Sharma, V., and Kumar, V. (2020). A short review on Rare earth doped NaYF<sub>4</sub> upconverted nanomaterials for solar cell applications. *Mater. Today Proc.* 21, 1868–1874. doi:10.1016/j.matpr.2020.01.243
- Kuriki, K., Koike, Y., and Okamoto, Y. (2002). Plastic optical fiber lasers and amplifiers containing lanthanide complexes. *Chem. Rev.* 102, 2347–2356. doi:10.1021/cr010309g
- Li, X., Yang, L., Zhu, Y., Zhong, J., and Chen, D. (2019). Upconversion of transparent glass ceramics containing β-NaYF<sub>4</sub>:Yb<sup>3+</sup>, Er<sup>3+</sup> nanocrystals for optical thermometry. *RSC Adv.* 9, 7948–7954. doi:10.1039/c9ra01088b
- Nicoli, F., Paltrinieri, E., Tranfić Bakić, M., Baroncini, M., Silvi, S., and Credi, A. (2021). Binary logic operations with artificial molecular machines. *Coord. Chem. Rev.* 428, 213589. doi:10.1016/j.ccr.2020.213589
- Nüchter, M., Ondruschka, B., Bonrath, W., and Gum, A. (2004). Microwave assisted synthesis – A critical technology overview. *Green Chem.* 6, 128–141. doi:10.1039/b310502d
- Piana, S., Reyhani, M., and Gale, J. D. (2005). Simulating micrometre-scale crystal growth from solution. *Nature* 438, 70–73. doi:10.1038/nature04173
- Sanna, S., Esposito, V., Andreasen, J. W., Hjelm, J., Zhang, W., Kasama, T., et al. (2015). Enhancement of the chemical stability in confined δ-Bi<sub>2</sub>O<sub>3</sub>. *Nat. Mat.* 14, 500–504. doi:10.1038/nmat4266
- Tanner, P. A. (2013). Some misconceptions concerning the electronic spectra of tri-positive europium and cerium. *Chem. Soc. Rev.* 42, 5090–5101. doi:10.1039/c3cs60033e
- Wang, C., Du, P., Li, W., and Luo, L. (2020a). Facile synthesis and photoluminescence performance of Er<sup>3+</sup>-activated BiOF sub-micro particles for ratiometric thermometers. *J. Lumin.* 226, 117416. doi:10.1016/j.jlumin.2020.117416
- Wang, C., Ran, W., Du, P., Li, W., Luo, L., and Wang, D. (2020b). Enhanced visible light-driven photocatalytic activities and photoluminescence characteristics of BiOF nanoparticles determined via doping engineering. *Inorg. Chem.* 59, 11801–11813. doi:10.1021/acs.inorgchem.0c01811
- Wang, X., Wang, Y., Jin, L., Bu, Y., Yang, X. L., and Yan, X. (2019). Controlling optical temperature detection of Ca<sub>3</sub>Al<sub>2</sub>O<sub>6</sub>: Yb<sup>3+</sup>, Er<sup>3+</sup> phosphors through doping. *J. Alloys Compd.* 773, 393–400. doi:10.1016/j.jallcom.2018.09.229
- Wei, J., Liu, Y., Zhang, M., Zheng, W., Huang, P., Gong, Z., et al. (2022). Blue-LED-excitable NIR-II luminescent lanthanide-doped SrS nanoprobe for ratiometric thermal sensing. *Sci. China Mat.* 65, 1094–1102. doi:10.1007/s40843-021-1801-8
- Xia, Y. N., Yang, P. D., Sun, Y. G., Wu, Y. Y., Mayers, B., Gates, B., et al. (2003). One-dimensional nanostructures: Synthesis, characterization, and applications. *Adv. Mat.* 15, 353–389. doi:10.1002/adma.200390087
- Xie, H.-H., Wen, Q., Huang, H., Sun, T.-Y., Li, P., Li, Y., et al. (2015). Synthesis of bright upconversion submicrocrystals for high-contrast imaging of latent fingerprints with cyanoacrylate fuming. *RSC Adv.* 5, 79525–79531. doi:10.1039/c5ra15255k
- Yi, G., Lu, H., Zhao, S., Ge, Y., Yang, W., Chen, D., et al. (2004). Synthesis, characterization, and biological application of size-controlled nanocrystalline NaYF<sub>4</sub>:Yb, Er infrared-to-visible up-conversion phosphors. *Nano Lett.* 4, 2191–2196. doi:10.1021/nl048680h
- Zaccariello, G., Back, M., Benedetti, A., Canton, P., Cattaruzza, E., Onoda, H., et al. (2019). Bismuth titanate-based UV filters embedded mesoporous silica nanoparticles: Role of bismuth concentration in the self-sealing process. *J. Colloid Interface Sci.* 549, 1–8. doi:10.1016/j.jcis.2019.04.042
- Zaccariello, G., Back, M., Zanella, M., Canton, P., Cattaruzza, E., Riello, P., et al. (2017). Formation and controlled growth of bismuth titanate phases into mesoporous silica nanoparticles: An efficient self-sealing nanosystem for UV filtering in cosmetic formulation. *ACS Appl. Mat. Interfaces* 9, 13252. doi:10.1021/acsami.6b13252
- Zanella, S., Hernández-Rodríguez, M. A., Carlos, L. D., Ferreira, R. A. S., and Brites, C. D. S. (2022). Reprogrammable and reconfigurable photonic molecular logic gates based on Ln<sup>3+</sup> ions. *Adv. Opt. Mat.* 10, 2200138. doi:10.1002/adom.202200138